Supplementary Information (SI) for Energy & Environmental Science.
This journal is © The Royal Society of Chemistry 2026

Supplementary Information

Estuarine-inspired dual-gradient hydrogel for stable and scalable moisture energy harvesting up to a single-module 100 mA output

Jie Miao, Haonan Wang*, Nan He, Bingsen Wang, Mengting Zhang, Dawei Tang, Lin Li*

Key Laboratory of Ocean Energy Utilization and Energy Conservation of Ministry of Education, School of Energy and Power Engineering, Dalian University of Technology, Dalian, 116024, People's Republic of China.

*Corresponding author: E-mail: wanghaonan@dlut.edu.cn (Haonan Wang), lilinnd@dlut.edu.cn (Lin Li)

Contents

Table S4 | The mass fraction of LiCl and Li_2CO_3 solution used for soaking i-vi types of DG-MEG.

Table S5 | Selection of control group and determination of the optimal range of ion concentration difference.

Table S6 | Voltage and current outputs of DG-MEG with active surface areas of 1, 10, 100, and 1000 cm^2.

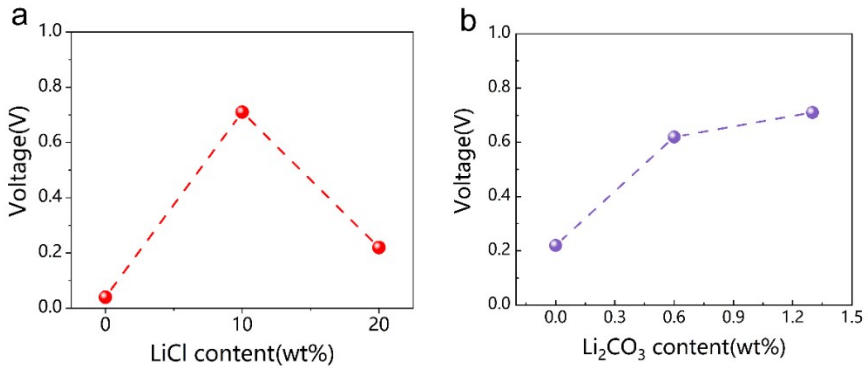

Fig. S1 Open circuit voltage of hydrogels with different hygroscopic salt concentrations a, Open-circuit voltage after impregnating a hygroscopic gel with different concentrations of lithium chloride (LiCl) solution. b, Open-circuit voltage after impregnating with desorption gel in different concentrations of lithium carbonate (Li_2CO_3) solution.

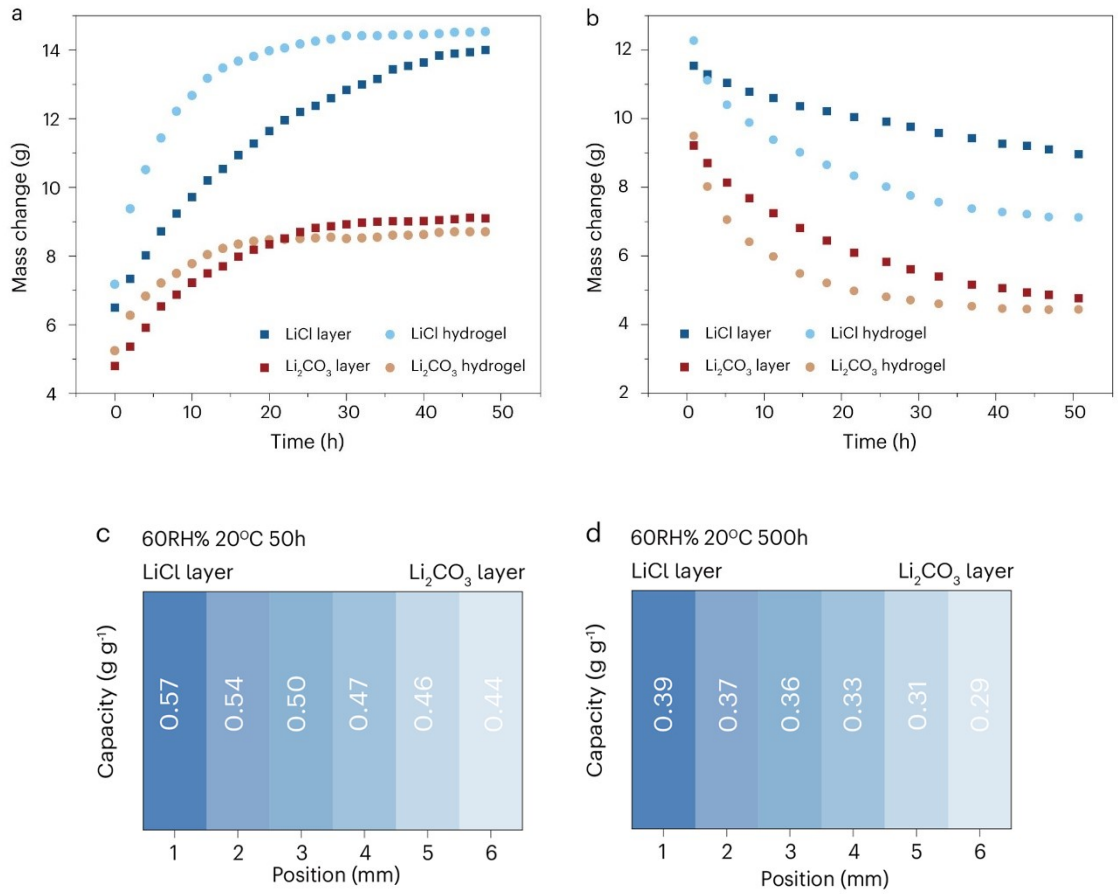

Fig. S2 Moisture content test of moisture absorbing layer. Moisture content of the absorbent layer during the water absorption process (a) and water loss process (b). Water mass content distribution at various positions within the DGH after 50 h (c) and 500 h (d) water absorption, confirming the presence of a stable water gradient.

In the water absorption stage, the LiCl layer absorbs more water faster than the Li_2CO_3 layer due to its stronger hygroscopicity, and this difference in hygroscopicity naturally forms an initial water gradient. When the two layers are coupled, the water absorbed by the LiCl layer continues to migrate towards the Li_2CO_3 layer, which significantly extends the saturation time of the LiCl layer from 15 hours when it exists alone to 50 hours. The Li_2CO_3 layer also extends its saturation time from 10 hours to 30 hours due to obtaining additional water supplementation to regulate the dynamic dissolution process. This directional flow directly delays the saturation process of the Li_2CO_3 layer. Even after reaching apparent saturation, the inherent difference in moisture absorption between the two layers will still maintain a gradient in water content, which ensures the stable existence of osmotic pressure difference. In the

dehydration experiment, the dehydration rate of the pre saturated double-layer system was reduced by 50% compared to the single-layer system, which directly proves the existence of continuous water transfer between the two layers: when the water in the Li_2CO_3 layer evaporates, the internal water gradient will automatically drive the LiCl layer to replenish the water in the Li_2CO_3 layer, forming a self-regulating mechanism.

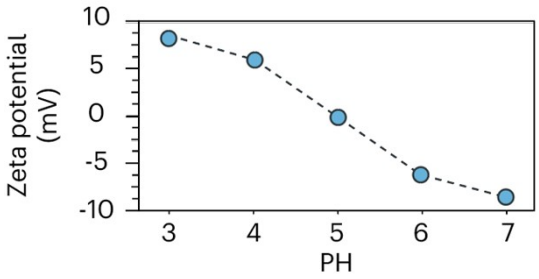

Fig. S3 Zeta potential of DGH in a pH range of 3 to 7.

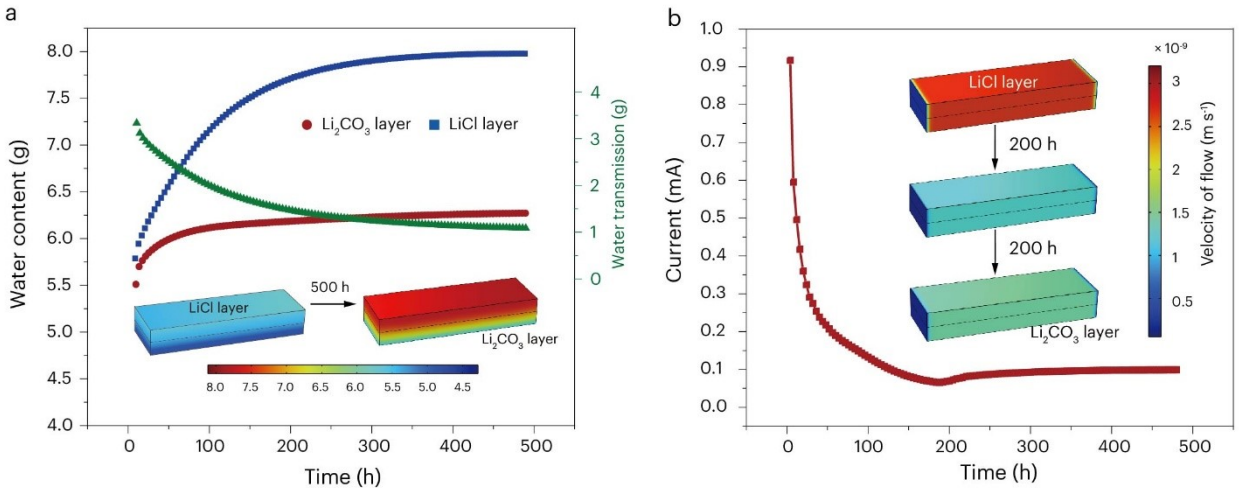

Fig. S4 Finite element simulation calculation of reverse transport process of water and ions. (a) Finite element simulation calculation of water transmission process. The red curve represents the change in water content of the Li_2CO_3 layer during equipment operation, the blue curve represents the change in water content of the LiCl layer, and the green curve represents the change in water transferred from the LiCl layer to the Li_2CO_3 layer, with the unit being grams. The color bands shown in the legend indicate the water content within the double-layer structure. (b) Finite element simulation calculation of current output and ion transport velocity. Finite element simulation calculation of current output and ion transport velocity. The built-in illustration shows that the ion transport speed between the two layers decreases from fast to slow and finally stabilizes, which is consistent with the trend of current output.

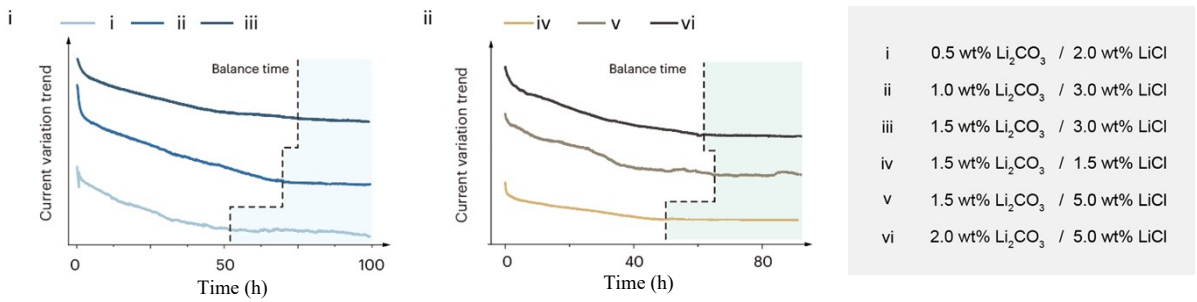

Fig. S5 Stability time of current of dual gradient hydrogel moisture electricity generator (DG-MEG) under different initial salt gradients. The initial salt gradient is achieved by immersing salt solutions of different concentrations.

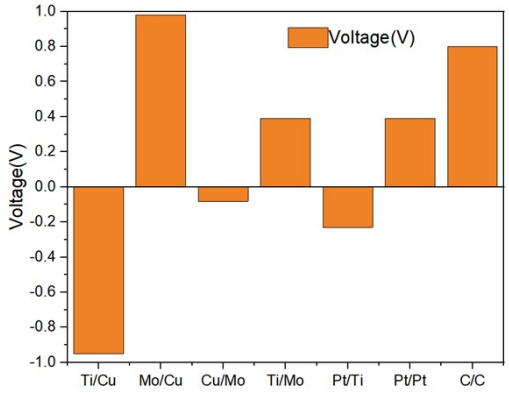

Fig. S6 The open-circuit voltage of the MEG with different electrode combinations. We conducted an in-depth exploration of the effects of different electrode materials on the performance of MEG, with a focus on evaluating a series of materials that are not easily reactive with water, such as Ti/Cu, Mo/Cu, Cu/Mo, Ti/Mo, Pt/Ti, Pt/Pt, and C/C, as positive and negative electrodes for their application in self-sustaining MEG. The MEG using traditional metal materials Ti/Mo as electrodes has an open circuit voltage of 0.4V. However, the open circuit voltage of MEG using C/C electrode material can reach 0.8V, indicating that carbon material electrodes can significantly improve the power generation efficiency of the MEG compared to traditional metal electrodes.

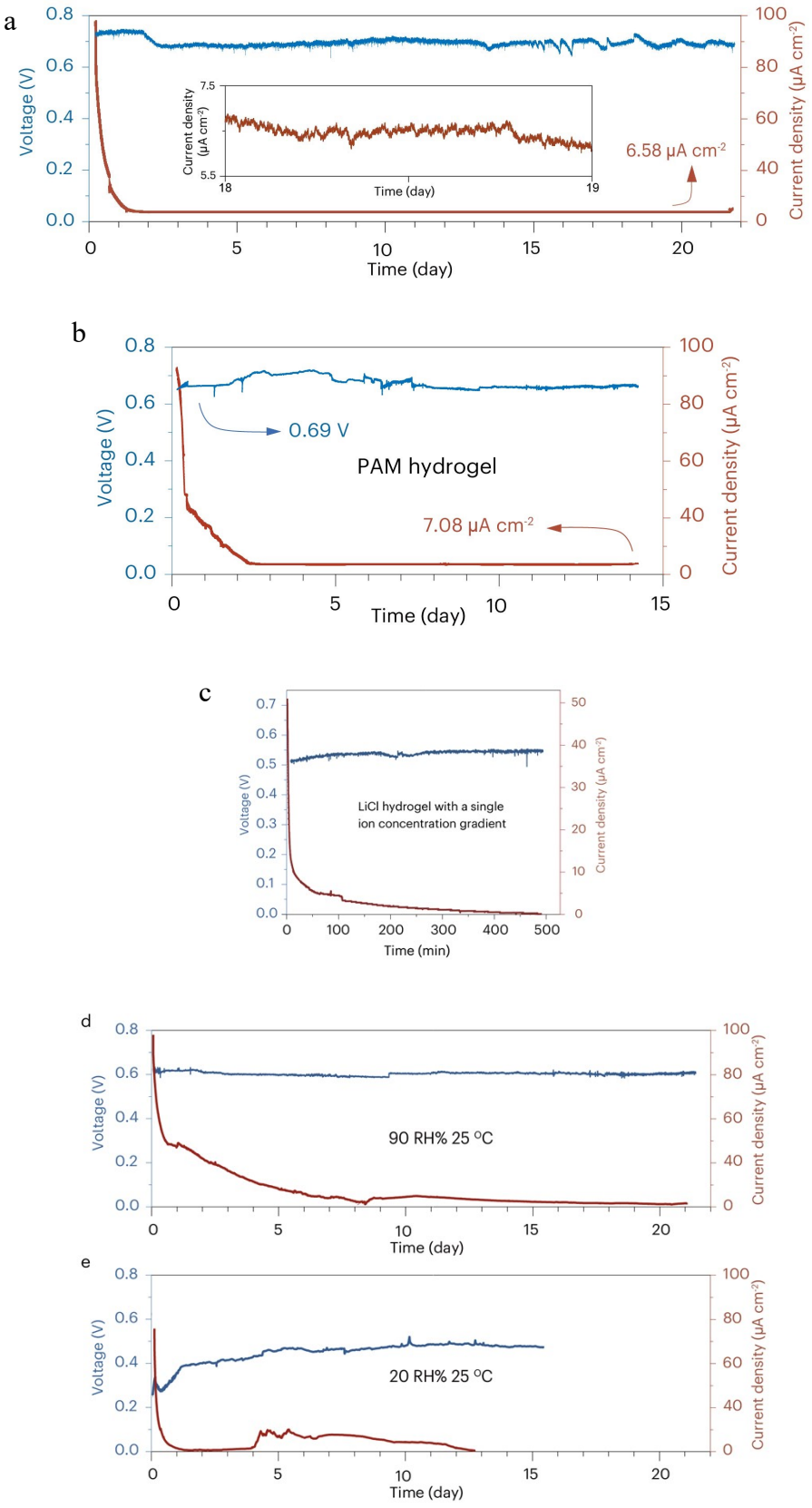

Fig. S7 Electrical performance output of power generation devices. (a) Continuous voltage and current density of DG-MEG operating under constant temperature and humidity conditions (25 °C,

60% RH). (b) Continuous voltage and current density of PAM hydrogel. (c) Electrical output performance of LiCl hydrogel with a single ion concentration gradient. (d) Continuous voltage and current density of DG-MEG operating at 25 ℃ and 90% RH. (e) Continuous voltage and current density of DG-MEG operating at 25 ℃ and 20% RH.

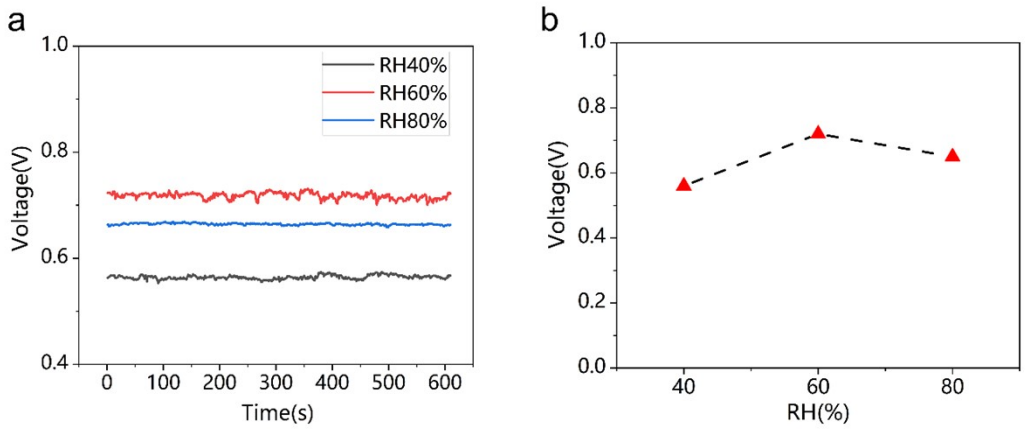

Fig. S8 Open-circuit voltages at different humidity. a, Open-circuit voltages at different humidity. b, Voltage trend with humidity.

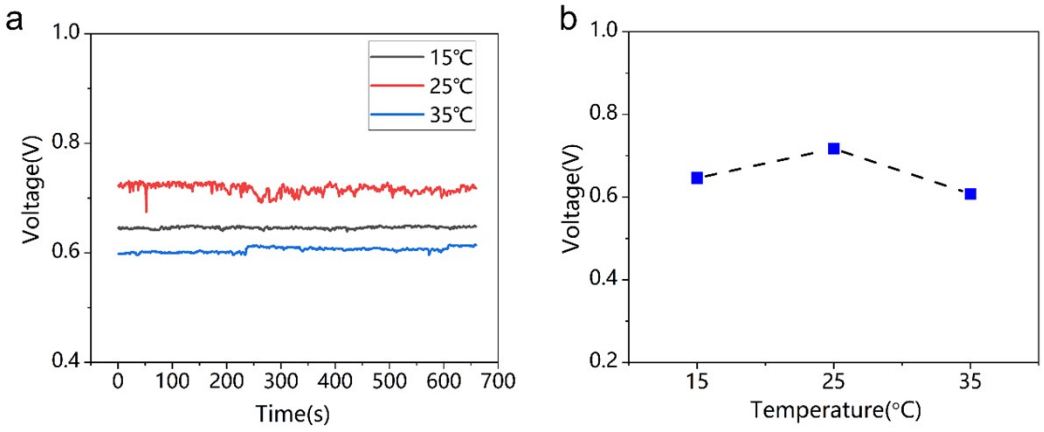

Fig. S9 The open-circuit voltage of the MEG at different temperatures. a, The open-circuit voltage of the MEG at different temperatures. b, The trend of the open-circuit voltage as a function of temperature.

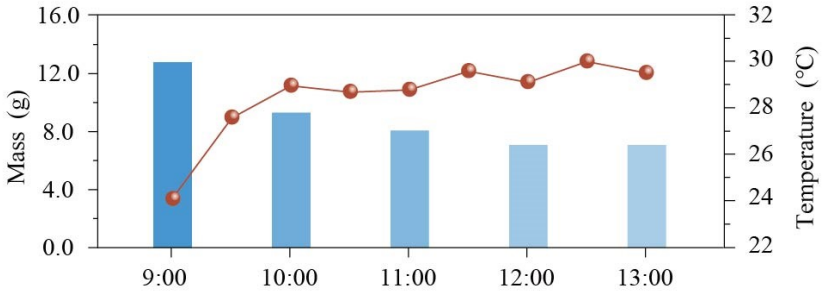

Fig. S10 Interface temperature and mass change of DG-MEG platform under 1-sun irradiation.

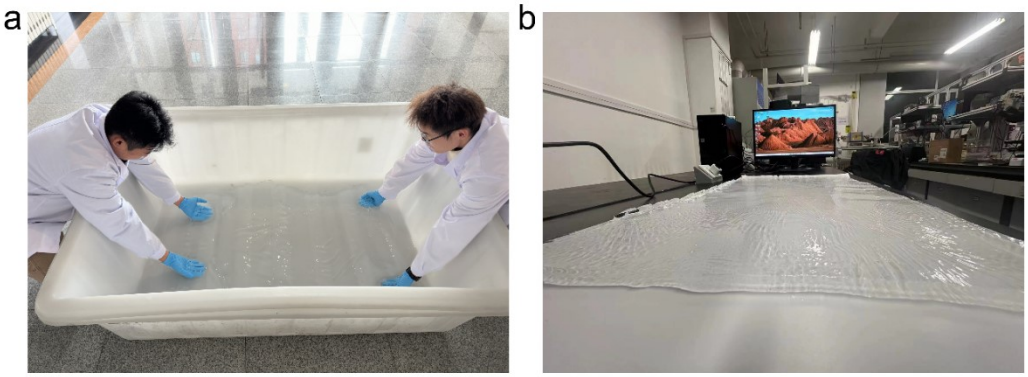

Fig. S11 Preparation of large size DGH. a, Preparation of the immersion step. b, Preparation of 1000 cm^2 ionic hydrogel.

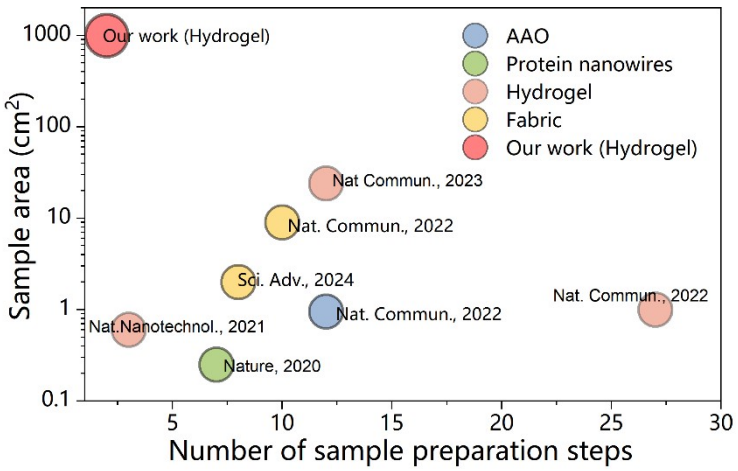

Fig. S12 Comparison of preparation area and number of preparation steps with works in the same field[1-7].

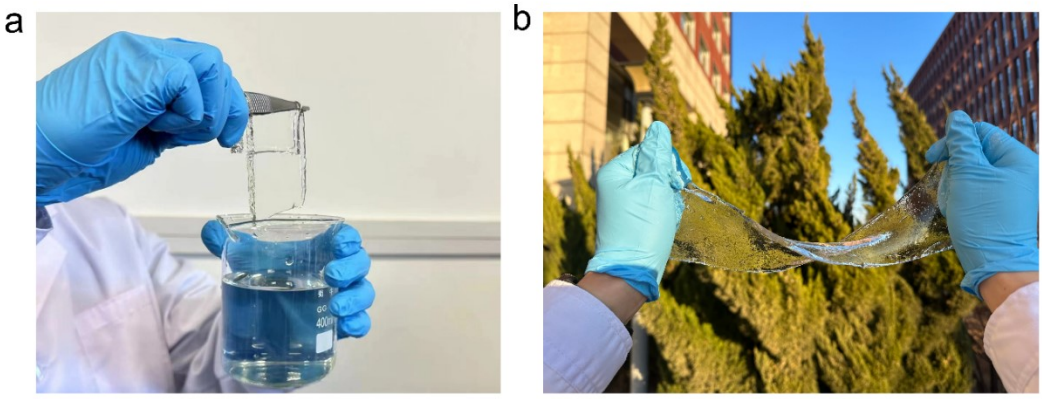

Fig. S13 Flexibility and transparency of DGH. a, Transparent properties of DGH. b, Flexibility of DGH.

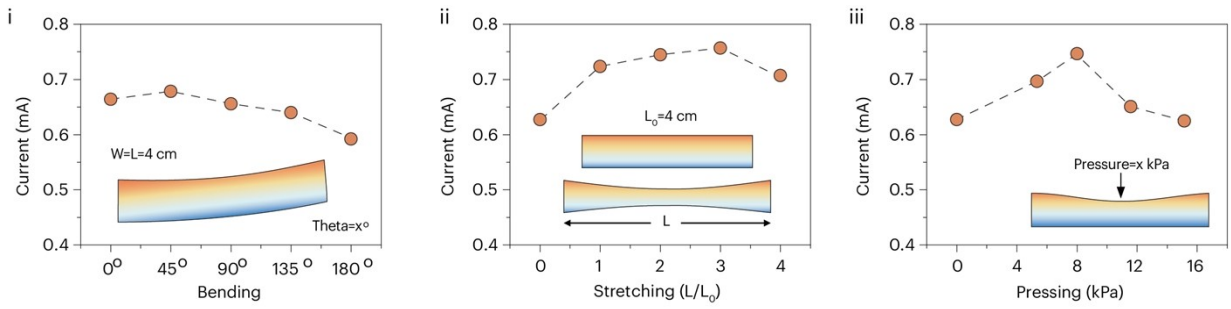

Fig. S14 Current output of DG-MEG under mechanical deformation, including bending, stretching, and compression.

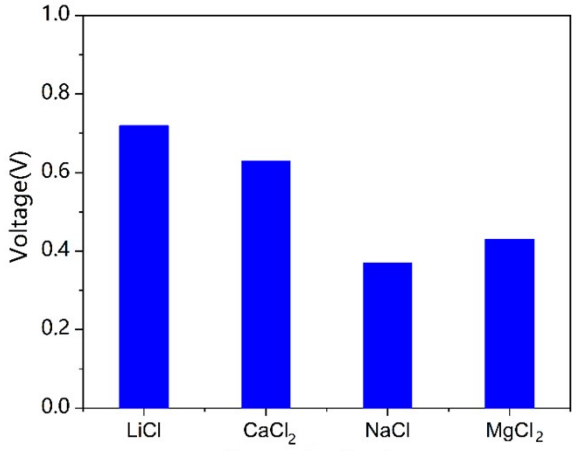

Fig. S15 Open-circuit voltage of a self-sustaining DG-MEG composed of hygroscopic gels impregnated with different hygroscopic salts.

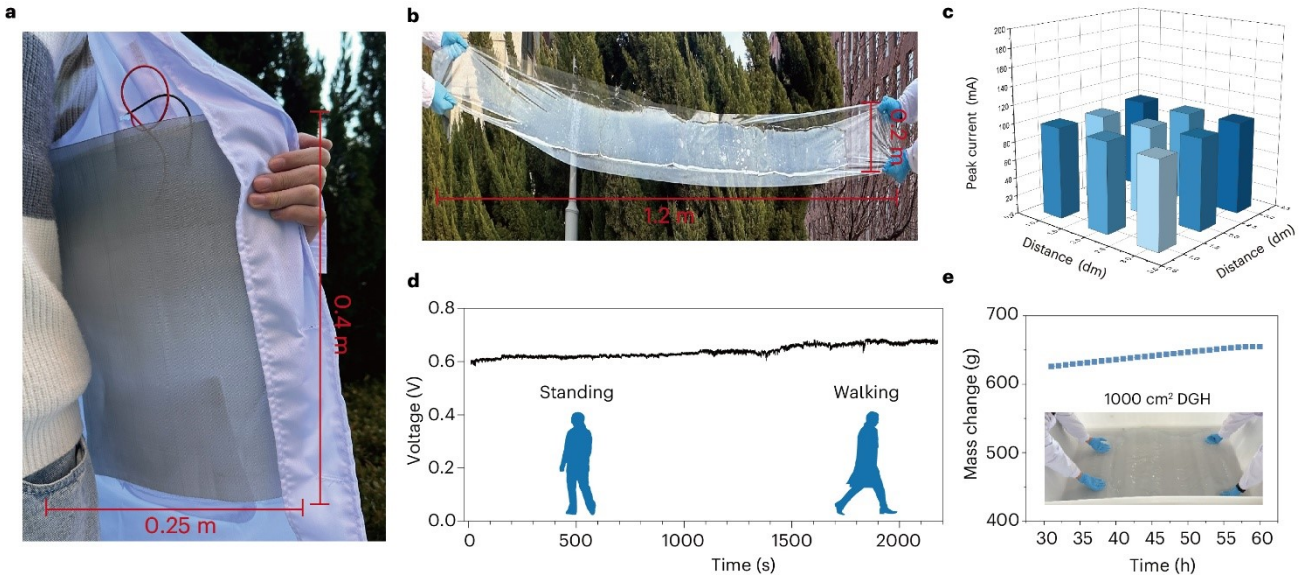

Fig. S16 (a) Large-sized DG-MEG exhibits long-term stability and reliability as a wearable power source. (b) Tensile testing of scalable large-sized DE-MEG. (c) Multi-point electrode detection of a square DE-MEG with a side length of 0.32m. (d) Stable electrical output of DG-MEG wearable energy source during walking and movement. (e) The mass change of 1000 cm^2 of DG-MEG after 30 hours of operation.

Table S1 Design and performance comparison of multi-layer moisture energy conversion equipment.

References	Strategy	Optimized gradient	Current density ($\mu A\ cm^{-2}$)	Duration (h)	Integrated method
Nat.Nanotechnol., 2021,16, 811–819	Asymmetric design of functional groups	Ion gradient	0.08	150	Series
*Adv.Mater.,*2022,34, 2201228	Asymmetric introduction of moisture	Water gradient	0.2-0.3	300	Series and parallel
Energy Environ. Sci., 2022, 15, 4584	Asymmetric design of functional groups	Ion gradient	1.3	120	Series and parallel
Energy Environ. Sci., 2024,17, 7165-7181	Asymmetric introduction of moisture	Water gradient	3-7	350	Series and parallel
Adv. Energy Mater., 2025, 2404840	Asymmetric introduction of moisture	Water gradient	2.52	100	Series
Our work	**Heterogeneous hygroscopic salt integration& Asymmetric introduction of moisture**	**Water gradient& Salinity gradient**	**7.23**	**500**	**Self-expansion &Series and parallel**

Table S2 Design and performance comparison of moisture energy conversion device

References	Strategy	Optimized gradient	Voltage (V)	Current density (μA cm^{-2})	Power density (μW cm^{-2})	Duration (h)	Integrated method
Nature, 2020, 578, 550	Asymmetric introduction of moisture	Water gradient	0.5	0.25	--	1500	Series and parallel
Nat.Nanotechnol., 2021 ,16, 811	Asymmetric design of functional groups	Ion gradient	1.38	0.9	5.52	250	Series
Nat.Commun., 2025,16, 5267	Asymmetric introduction of moisture	Water gradient	0.45-0.6	--	12.43	240	Series and parallel
Nat. Commun., 2024, 15, 4929	Asymmetric design of functional groups	Ion gradient	0.87	2-3	--	120	Series and parallel
Adv. Mater., 2022,34, 2201228	Asymmetric introduction of moisture	Water gradient	0.8	0.2-0.3	35	300	Series and parallel
Energy Environ. Sci., 2022, 15, 4584	Asymmetric design of functional groups	Ion gradient	0.7	1.3	0.15	120	Series and parallel
Energy Environ. Sci., 2024,17, 7165	Asymmetric introduction of moisture	Water gradient	0.703	3-7	28.9	350	Series and parallel
Adv. Energy Mater., 2025, 2404840	Asymmetric introduction of moisture	Water gradient	1.25	2.52	0.78	100	Series

Adv. Mater., 2024, 36, 2208081	Asymmetric introduction of moisture	Water gradient	0.6	0.83-0.90	0.5-0.54	120	Series and parallel
Energy Environ. Sci., 2023, 10, 4577	Asymmetric design of functional groups	Ion gradient	0.7	3	0.15	120	Series and parallel
Energy Environ. Sci., 2019, 12, 1848	Asymmetric introduction of moisture	Water gradient	0.6	1.2	0.07	120	Series and parallel
ACS Appl. Mater. Interfaces, 2025, 17, 1944	Asymmetric design of functional groups	Ion gradient	1.03	--	9.12	168	Series and parallel
ACS Appl. Mater. Interfaces, 2022, 14, 19569	Asymmetric design of functional groups	Ion gradient	1	8.2	2.2	74	Series
Adv. Funct. Mater., 2019, 29, 2204627	Asymmetric introduction of moisture	Water gradient	0.1	0.02	0.0003	167	Series and parallel
Chem. Eng. J., 2024, 486, 150203	Asymmetric design of functional groups	Ion gradient	0.67	6.4	0.87	70	Series and parallel
Adv Funct Mater. 2023, 33, 2210027	Asymmetric design of functional groups	Ion gradient	1.9	--	22.5	5	Series and parallel
Green Energy Environ., *DOI:10.1016/j.gee.2025.05.004*	Asymmetric introduction of moisture	Water gradient	0.39	--	14.87	720	Series and parallel

Adv. Energy Mater., 2024, 14, 240637	Asymmetric introduction of moisture	Water gradient	1.08	36.8	5.83	24	Series and parallel
ACS Nano, 2024, 18, 12096	Asymmetric introduction of moisture	Water gradient	0.4	5.7	--	3	Series and parallel
Our work	**Heterogeneous hygroscopic salt integration& Asymmetric introduction of moisture**	**Water gradient& Salinity gradient**	**0.7**	**7.23**	**5.06 (after 500 power supply)**	**500**	**Self-expansion &Series and parallel**

Table S2 (appendix) Design and performance comparison of moisture energy conversion device

References	Voltage (V)	Current density (mA cm^{-2})	Power density (mW cm^{-2})	Duration (h)	Strategy
Adv. Mater. 2025, e15133.	1.44	4.6	0.59	400	Water gradient and active electrode system
Energy Environ. Sci. 2025, 18, 9457	0.6	0.58	0.088	288	Conductive nanochannels and asymmetric electrodes
ACS Appl. Mater. Interfaces 2025, 17, 7916	1.03	0.0238	0.00912	168	Hydrogel-aerogel double-layer structure
Interdiscip. Mater. 2025, 4, 869	0.9-1.25	0.539	0.124	200	Introduction of ionic liquids and active electrodes
ACS Nano 2025, 19, 3807	0.8	0.0645	0.021	100	Hydrogel array combined with double-layer pseudocapacitance model
Chem. Eng. J. 2025, 511, 162246.	0.95	0.113	0.106	—	Humidity gradient and asymmetric active electrode
Our work	**0.7**	**0.096**	**0.005**	**500**	**Osmotic pressure regulation and dual gradient driving**

Table S3 Changes in Li^+ concentration before and after electrical output testing

DG-MEG	Concentration of Li+ in LiCl layer ($\mu g\ mL^{-1}$)		Concentration of Li+ in Li_2CO_3 layer ($\mu g\ mL^{-1}$)	
	Before testing	After testing	Before testing	After testing
i	96.5	162.5	231.9	181.7
ii	94	123.5	292.1	159.9
iii	95.2	134.7	352.4	203.8
iv	34.6	94.4	161.5	95.6
v	90.3	197.4	398.6	229.8
vi	127.5	175.9	282.7	194.6

Table S4 The mass fraction of LiCl and Li_2CO_3 solution used for soaking i-vi types of DG-MEG

Type of DG-MEG	Mass fraction of LiCl immersion solution	Mass fraction of Li_2CO_3 immersion solution	Concentration of Li^+ in LiCl layer (μg mL^{-1})	Concentration of Li^+ in Li_2CO_3 layer (μg mL^{-1})
i	2.0 wt%	0.5 wt%	96.5	231.9
ii	3.0 wt%	1.0 wt%	94	292.1
iii	3.0 wt%	1.5 wt%	95.2	352.4
iv	1.5 wt%	1.5 wt%	34.6	161.5
v	5.0 wt%	1.5 wt%	90.3	398.6
vi	5.0 wt%	2.0 wt%	127.5	282.7

Table S5 Selection of control group and determination of the optimal range of ion concentration difference

Δ C ($\mu g\ mL^{-1}$)	Mass fraction of LiCl immersion solution	Mass fraction of Li_2CO_3 immersion solution	Concentration of Li^+ in LiCl layer ($\mu g\ mL^{-1}$)	Concentration of Li^+ in Li_2CO_3 layer ($\mu g\ mL^{-1}$)	Voltage (V)
257.2	3.0 wt%	1.5 wt%	95.2	352.4	0.78
249.4	3.5 wt%	1.5 wt%	93.8	343.2	0.72
268.9	4.0 wt%	1.5 wt%	90.6	359.5	0.81
286.3	4.5 wt%	1.5 wt%	91.3	377.6	0.64
308.3	5.0 wt%	1.5 wt%	90.3	398.6	0.52

Table S6 Voltage and current outputs of DG-MEG with active surface areas of 1, 10, 100, and 1000 cm^2

Area (cm^2)	Voltage (V)	Current (mA)
1	0.67	0.0958
10	0.73	0.8334
100	0.64	9.0975
1000	0.68	102.384

References

1. Liu, X. et al. Power generation from ambient humidity using protein nanowires. *Nature*, **578**, 550-554 (2020).
2. Hu, Y. et al. Phyto-inspired sustainable and high- performance fabric generators via moisture absorption-evaporation cycles. *Sci. Adv.*, 2024, **10**, 4620.
3. Tan, J. et al. Self-sustained electricity generator driven by the compatible integration of ambient moisture adsorption and evaporation. *Nat Commun.*, 2022, **13**, 3643.
4. Yang, S. et al. Green moisture-electric generator based on supramolecular hydrogel with tens of milliamp electricity toward practical applications. *Nat. Commun.*, 2024, **15**, 3329.
5. Wang, H. et al. Bilayer of polyelectrolyte films for spontaneous power generation in air up to an integrated 1,000 V output. *Nat. Nanotechnol.*, 2021, **16**, 811-819.
6. Zhang, Y. et al. Sustainable power generation for at least one month from ambient humidity using unique nanofluidic diode. *Nat. Commun.*, 2022, **13**, 542-548.
7. Liu, X. et al. Microbial biofilms for electricity generation from water evaporation and power to wearables. *Nat. Commun.*, 2022, **13**, 4369.
8. Wang, R. et al. High-performance moisture-driven power generators based on in-situ confined polymerized ionic liquid membranes. *Green Energy Environ.*, 2025, Advance Article. https://doi.org/10.1016/j.gee.2025.05.004
9. Guo, S. et al. Leaf-based energy harvesting and storage utilizing hygroscopic iron hydrogel for continuous power generation. *Nat. Commun.*, 2025, **16**, 5267.
10. He, W. et al. Robustly and Intrinsically Stretchable Ionic Gel-Based Moisture-Enabled Power Generator with High Human Body Conformality. *ACS Nano*, 2024, **18**, 12096-12104.
11. Sun, Z. et al. Capacitor-inspired high-performance and durable moist-electric generator. *Energy Environ. Sci.*, 2022, **15**, 4584.

12. Shin, E. et al. Environmentally sustainable moisture energy harvester with chemically networked cellulose nanofiber. *Energy Environ. Sci.*, 2024, **17**, 7165-7181.

13. Zhang, K. et al. Simulating solid electrolyte interphase formation spanning 108 time scales with an atomically informed phase-field model. *Energy Environ. Sci.*, 2025, **18**, 7541-7554.

14. Huang, H. et al. All-region-applicable, continuous power supply of graphene oxide composite. *Energy Environ. Sci.*, 2019, **12**, 1848.

15. Zhong, H. et al. Asymmetric self-powered cellulose-based aerogel for moisture-electricity generation and humidity sensing. *Chem. Eng. J.*, 2024, **486**, 150203.

16. Wu, Y. et al. A Hygroscopic Janus Heterojunction for Continuous Moisture Triggered Electricity Generators. *ACS Appl. Mater. Interfaces*, 2022, **14**, 19569-19578.

17. Huang, Z. et al. Flexible Moisture-Driven Electricity Generators Based on Heterogeneous Gels and Carbon Nanotubes. *ACS Appl. Mater. Interfaces*, 2025, **17**, 7916-7928.

18. Wang, L. et al. Moisture-enabled self-charging and voltage stabilizing supercapacitor. *Nat. Commun.*, 2024, **15**, 4929.

19. Zhang, Y. et al. An Asymmetric Hygroscopic Structure for Moisture-Driven Hygro-Ionic Electricity Generation and Storage. *Adv. Mater.*, 2022, **34**, 2201228.

20. Zhang, X. et al. Biomimetic Aerogel for Moisture-Induced Energy Harvesting and Self-Powered Electronic Skin. *Adv. Funct. Mater.*, 2023, **33**, 2210027.

21. Zhou, J. et al. Bioinspired Interfacial Design of Robust Aramid Nanofiber Composite Films for High-Performance Moisture-Electric Generators. *Adv. Energy Mater.*, 2025, **15**, 2404840.

22. Tian, K. et al. Evaporation-Induced Closely-Packing of Core-Shell PDMS@Ag Microspheres Enabled Stretchable Conductor with Ultra-High Conductance. *Adv. Funct. Mater.*, 2023, **33**, 2308799.